Supporting Information

Tuning local Lewis acidity in transition-metal-doped Nb_2C MXenes for enhanced urea electrosynthesis

Lianming Zhao,* Yuan Li,[a] Xueru Wang,[a] Wenxi Han,[a] Jinghao Zhang,[a] Jifa Fu,[a] Yuqi Qiu,[a] Xiaojie Liu,[a] Wenxuan An,[a] Zhanchi Zhao,[a] GuangZhao,[b] Wei Xing[a] and Jing Xu*[a]

[a] Shandong Key Laboratory of Intelligent Energy Materials, School of Materials Science and Engineering, China University of Petroleum (East China), Qingdao, Shandong 266580, China

[b] School of Petroleum Engineering, China University of Petroleum (East China), Qingdao, Shandong 266580, China

*Corresponding authors.

E-mail addresses: lmzhao@upc.edu.cn (L. Zhao), and xujing@upc.edu.cn (J. Xu).

Table of contents

Computational details

Fluoride ion affinity (FIA) serves as a quantitative descriptor for Lewis acidity. It was defined as the negative enthalpy change (−ΔH) associated with the binding of a Lewis acid (LA) to a fluoride ion (F^-), calculated as:

$$\text{FIA} = -\Delta H = -(\Delta E + \Delta ZPE) \quad (1)$$

where ΔE is the total energy difference and ΔZPE is the zero-point energy correction.

To evaluate the fluoride-binding capability of LA, we employed hydrogen fluoride (HF) as an indirect probe and examined the following exchange reactions:

$$\text{LA} + \text{HF} \rightarrow [\text{LA - F}]^- + \text{H}^+ \quad (2)$$

$$\text{H}^+ + \text{F}^- \rightarrow \text{HF} \quad (3)$$

$$\text{LA} + \text{F}^- \rightarrow [\text{LA - F}]^- \quad (4)$$

Summing Eqs. (2) and (3) yields the net reaction shown in Eq. (4), which represents the direct interaction between the Lewis acid and the fluoride ion.

To enhance the reliability of the FIA values, we prioritized solvated-phase results over gas-phase ones. The relevant solvation processes were defined as:

$$\text{HF(g)} \rightarrow \text{HF(aq)} \quad (5)$$

$$\text{H}^+\text{(aq)} \rightarrow \text{H}^+\text{(g)} \quad (6)$$

$$\text{F}^-\text{(aq)} \rightarrow \text{F}^-\text{(g)} \quad (7)$$

$$\text{H}^+\text{(g)} + \text{F}^-\text{(g)} \rightarrow \text{HF(g)} \quad (8)$$

$$\text{H}^+\text{(aq)} + \text{F}^-\text{(aq)} \rightarrow \text{HF(aq)} \quad (9)$$

The enthalpy change for Eq. (9) was determined by summing the values for Eqs. (5–8). Based on standard-state thermochemical data at 298.15 K and 1 atm, the individual enthalpy changes are: $\Delta H_5 = -47$ kJ mol^{-1},[1] $\Delta H_6 = 1091$ kJ mol^{-1}, $\Delta H_7 = 515$ kJ mol^{-1},[2] $\Delta H_8 = -1555$ kJ mol^{-1}.[3] Consequently, the net enthalpy change for Eq. (9) was calculated as: $\Delta H_9 = \Delta H_5 + \Delta H_6 + \Delta H_7 + \Delta H_8 = 4$ kJ mol^{-1}. This small positive value indicates that the solvation process described in Eq. (9) is slightly endothermic.

Therefore, the solvated fluoride ion affinity ($FIA_{solv}^{TM@Nb_2C}$) at the TM site on TM@Nb_2C was calculated as:

$$FIA_{solv}^{TM@Nb_2C} = -\left(\Delta H_2^{TM@Nb_2C} + \Delta H_9\right) \tag{10}$$

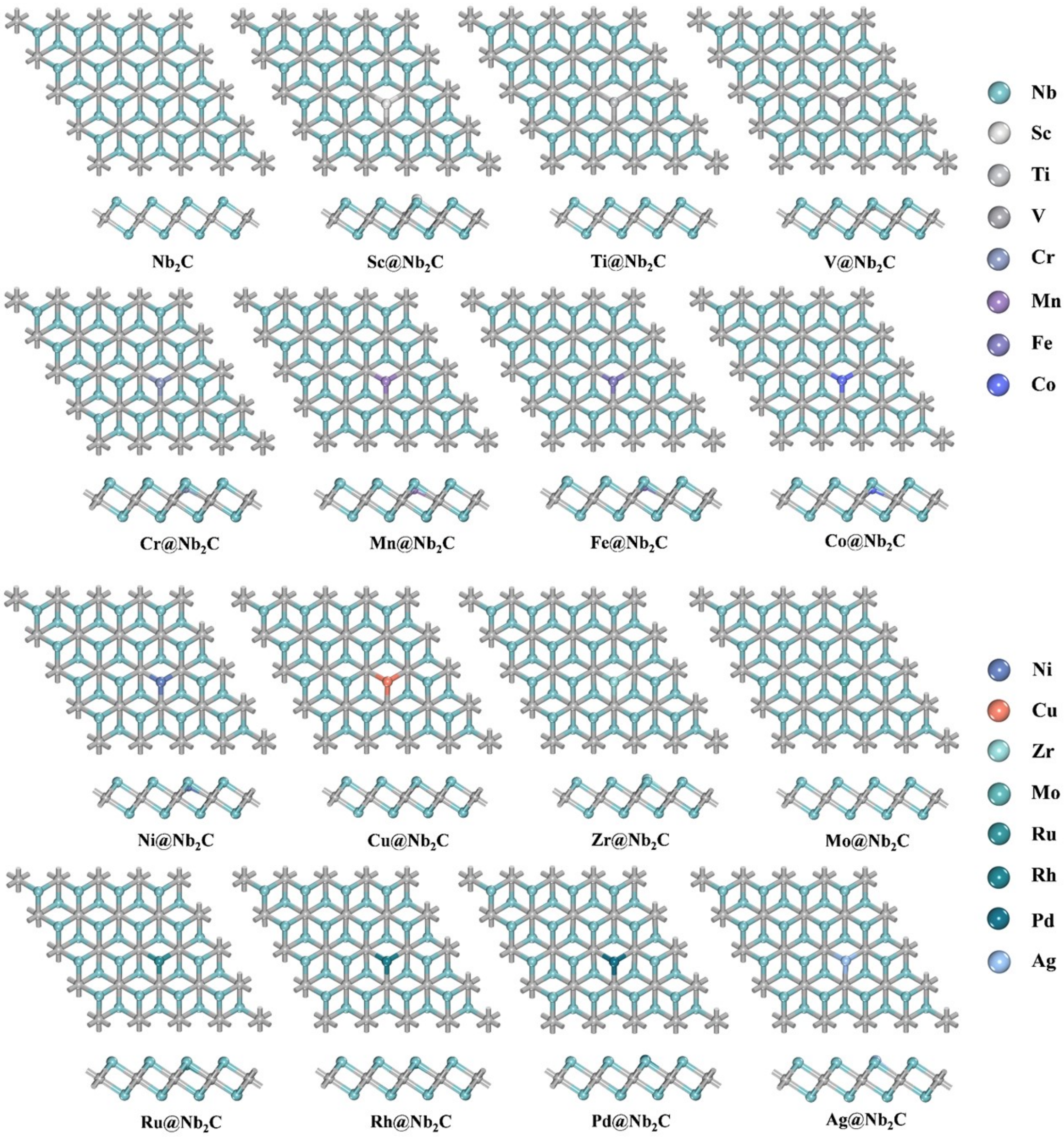

Fig. S1 Top and side views of the optimized structure of Nb_2C and TM@Nb_2C.

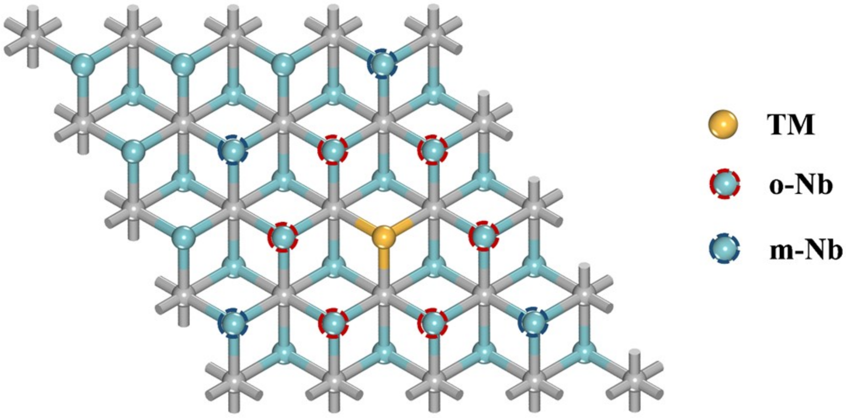

Fig. S2 Schematic illustration of Nb sites at varying distances from the TM dopant in TM@Nb_2C for charge (acidity) gradient analysis. The TM atom is highlighted in gold. Nb atoms in the nearest proximity to the TM site are denoted as o-Nb (red dashed circles), while those in the next-nearest positions are denoted as m-Nb (blue dashed circles).

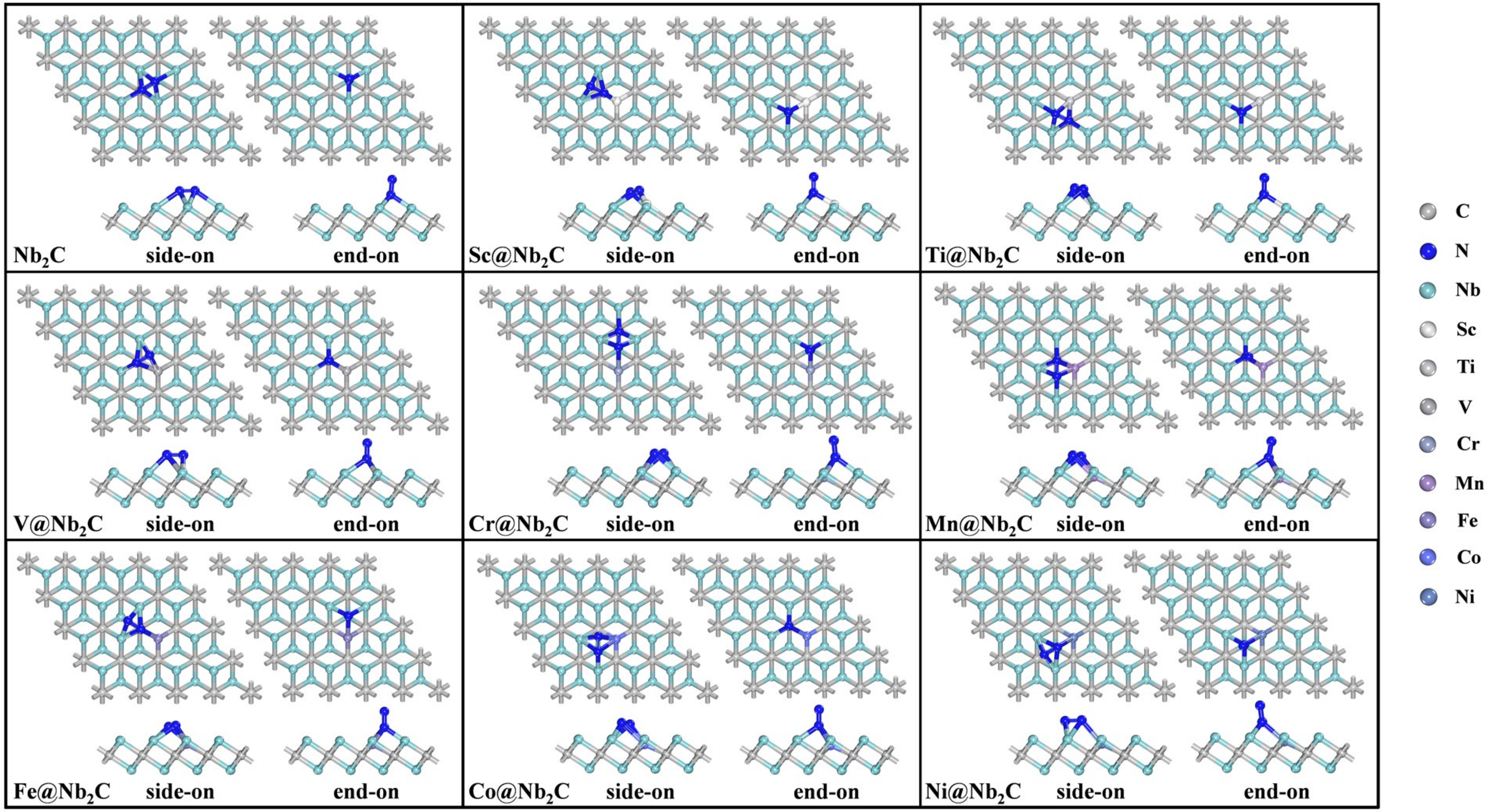

Fig. S3 Top and side views of the optimized adsorption configurations for N_2 on Nb_2C and TM@Nb_2C (TM = Sc, Ti, V, Cr, Mn, Fe, Co, and Ni).

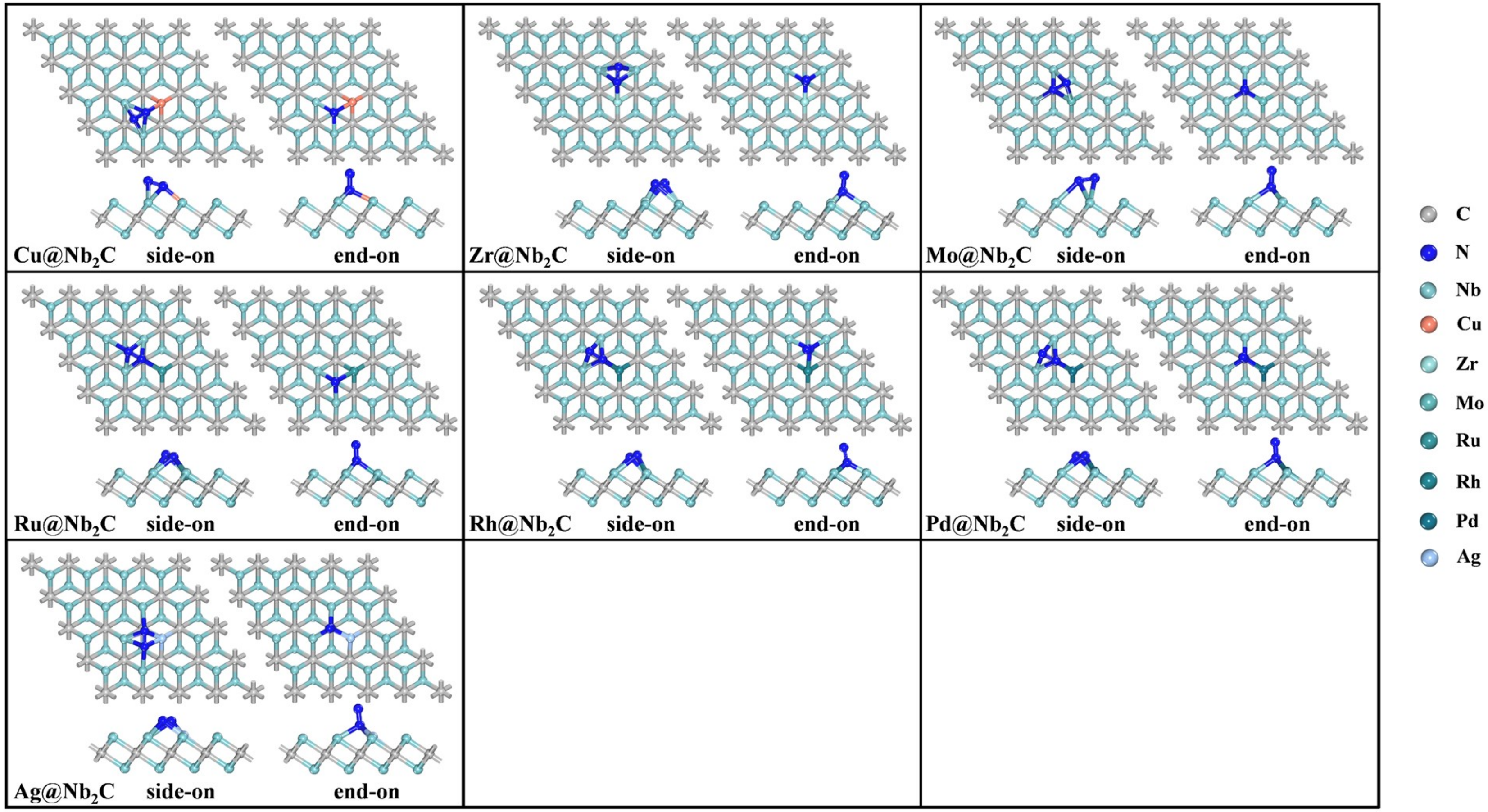

Fig. S4 Top and side views of the optimized adsorption configurations for N_2 on TM@Nb_2C (TM = Cu, Zr, Mo, Ru, Rh, Pd, and Ag).

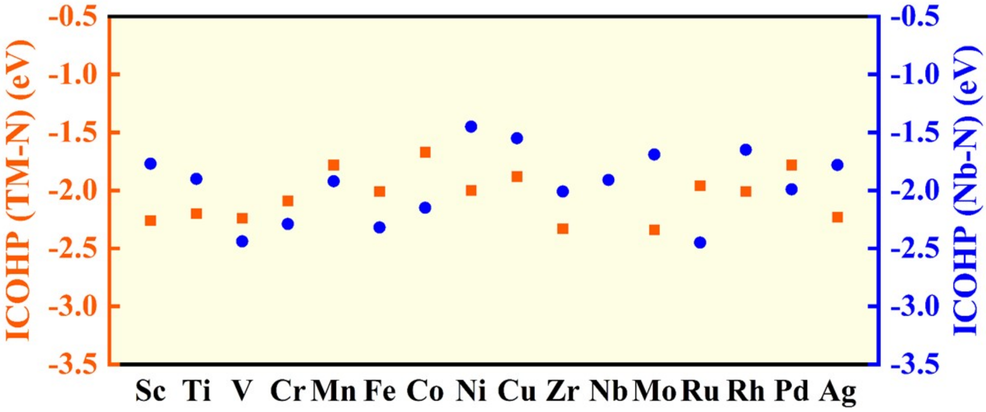

Fig. S5 Mean ICOHP values for the side-on adsorbed N_2 on Nb_2C and TM@Nb_2C. Orange squares represent the mean ICOHP of TM–N bonds (left y-axis), and blue circles represent the mean ICOHP of Nb–N bonds (right y-axis). For pristine Nb_2C, TM–N bonds are absent.

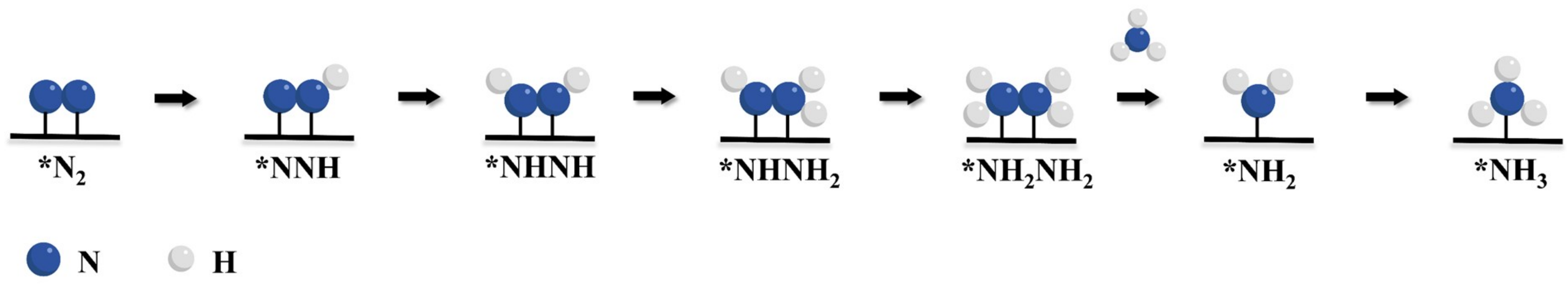

Fig. S6 Schematic illustration of the NRR process.

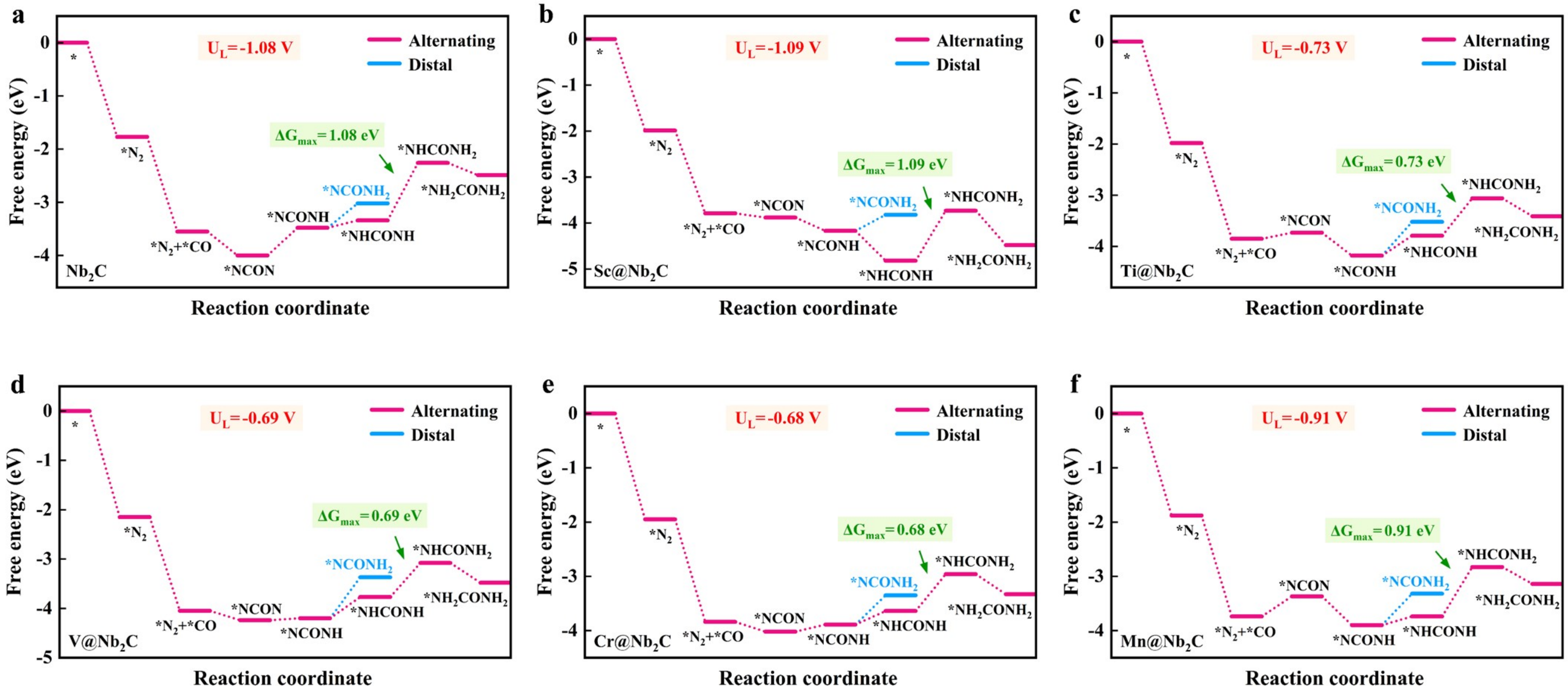

Fig. S7 Free energy diagrams for urea electrosynthesis on (a) Nb_2C, (b) Sc@Nb_2C, (c) Ti@Nb_2C, (d) V@Nb_2C, (e) Cr@Nb_2C, and (f) Mn@Nb_2C.

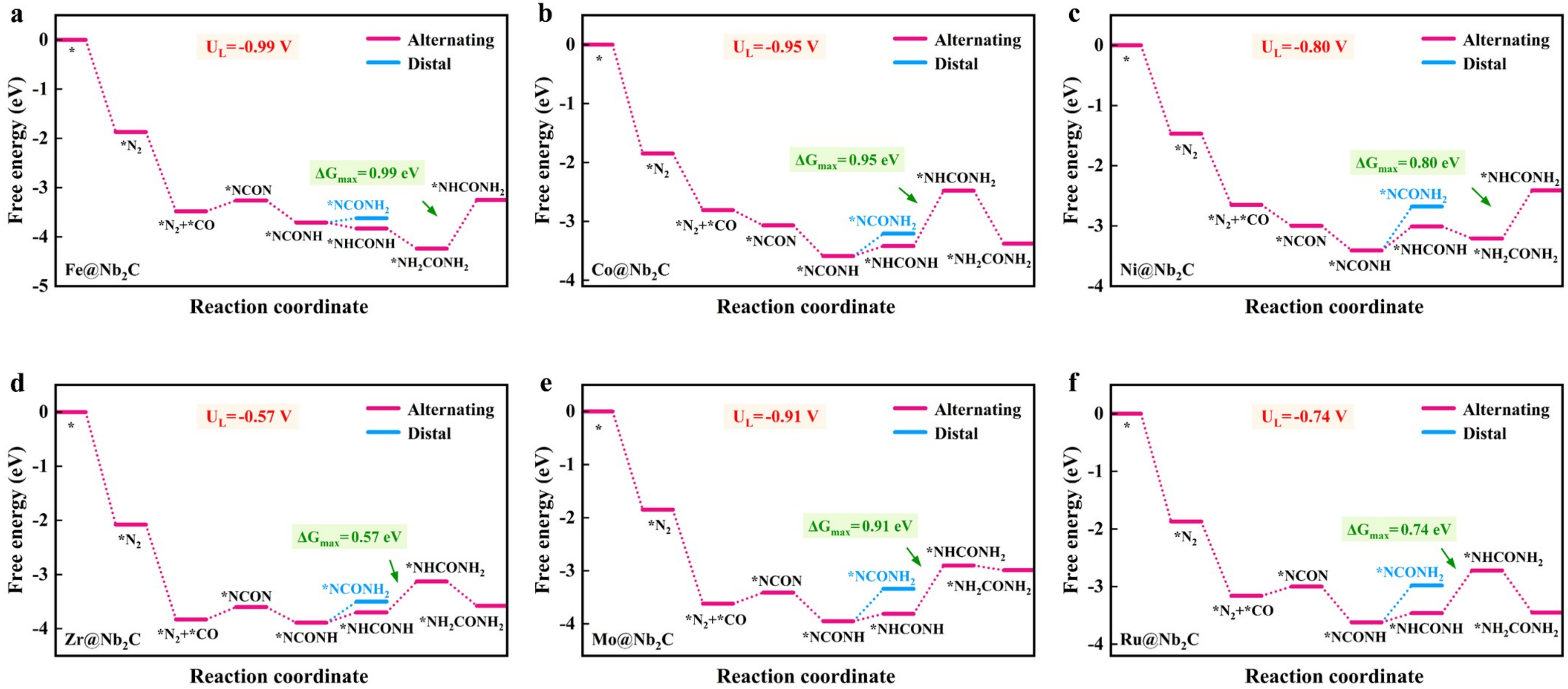

Fig. S8 Free energy diagrams for urea electrosynthesis on (a) Fe@Nb_2C, (b) Co@Nb_2C, (c) Ni@Nb_2C, (d) Zr@Nb_2C, (e) Mo@Nb_2C, and (f) Ru@Nb_2C.

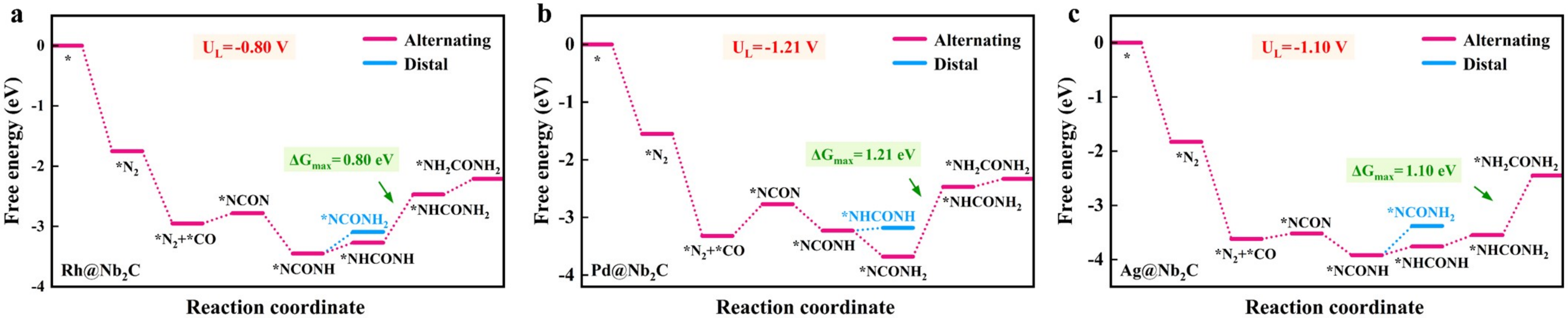

Fig. S9 Free energy diagrams for urea electrosynthesis on (a) Rh@Nb_2C, (b) Pd@Nb_2C, and (c) Ag@Nb_2C.

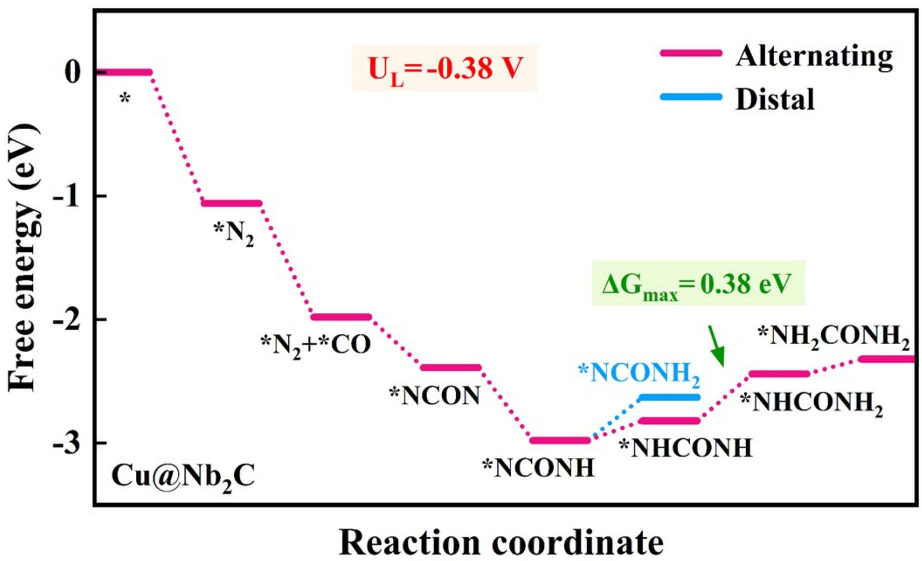

Fig. S10 Free energy diagram for urea electrosynthesis on Cu@Nb_2C including solvent effects.

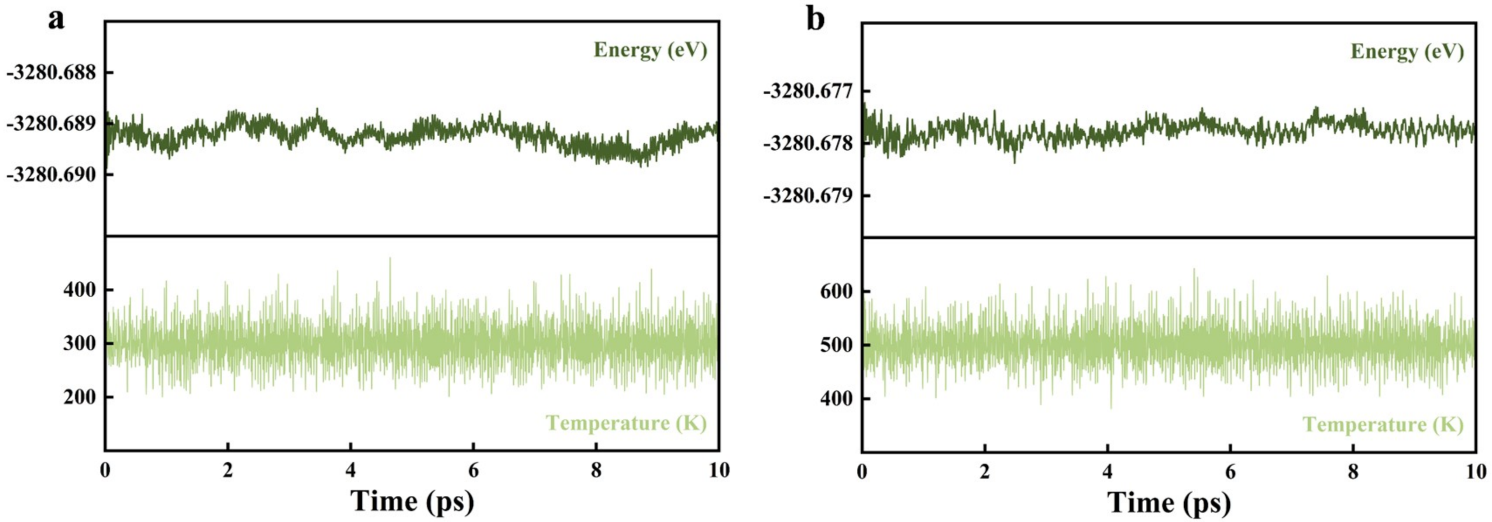

Fig. S11 AIMD simulations of Cu@Nb_2C (a) at 300 K and (b) 500 K.

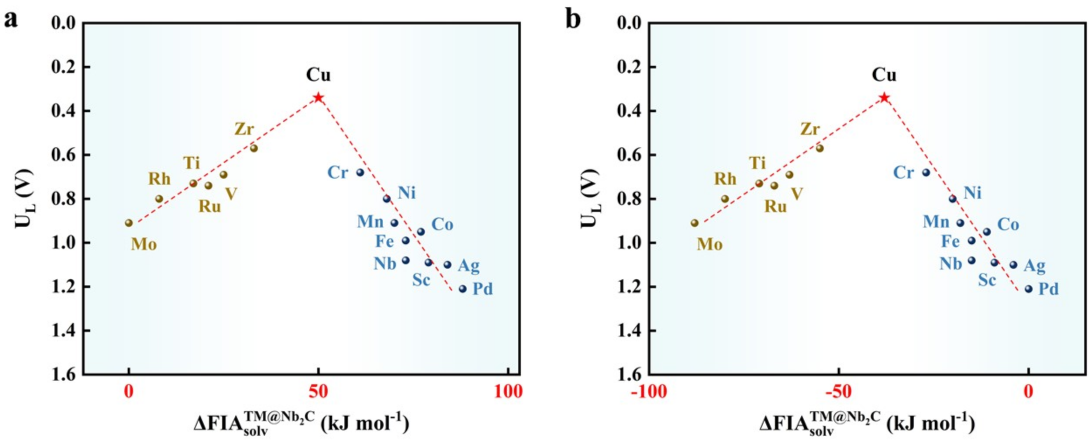

Fig. S12 Volcano plot showing the relationship between the solvation-corrected relative fluoride ion affinity ($\Delta FIA_{solv}^{TM@Nb_2C}$) and the limiting potential for urea synthesis (U_L), with the reference zero set to the solvated fluoride ion affinity of (a) Mo@Nb_2C and (b) Pd@Nb_2C.

Table S1. Calculated Hirshfeld charges (|e|) for the TM dopant site, and the average charges of the o-Nb and m-Nb sites on Nb_2C and TM@Nb_2C.

System	q(TM)	q(o-Nb)	q(m-Nb)
Nb_2C	0.546	0.546	0.546
Sc@Nb_2C	0.260	0.478	0.544
Ti@Nb_2C	0.149	0.463	0.568
V@Nb_2C	0.254	0.548	0.556
Cr@Nb_2C	0.279	0.550	0.552
Mn@Nb_2C	0.175	0.548	0.556
Fe@Nb_2C	0.166	0.525	0.556
Co@Nb_2C	0.164	0.508	0.559
Ni@Nb_2C	0.139	0.494	0.560
Cu@Nb_2C	0.112	0.497	0.560
Zr@Nb_2C	0.199	0.394	0.527
Mo@Nb_2C	0.105	0.550	0.600
Ru@Nb_2C	0.149	0.536	0.558
Rh@Nb_2C	0.105	0.565	0.582
Pd@Nb_2C	0.144	0.545	0.570
Ag@Nb_2C	0.286	0.539	0.572

Table S2. Calculated adsorption energy (eV) of $^*N_2$ on Nb_2C and TM@Nb_2C.

System	Side on	End on
Nb_2C	-2.22	-1.10
Sc@Nb_2C	-2.55	-1.07
Ti@Nb_2C	-2.57	-1.08
V@Nb_2C	-2.71	-1.11
Cr@Nb_2C	-2.66	-1.12
Mn@Nb_2C	-2.30	-1.12
Fe@Nb_2C	-2.62	-0.94
Co@Nb_2C	-2.47	-1.12
Ni@Nb_2C	-1.91	-1.11
Cu@Nb_2C	-1.96	-0.99
Zr@Nb_2C	-2.63	-1.07
Mo@Nb_2C	-2.34	-1.11
Ru@Nb_2C	-2.39	-1.11
Rh@Nb_2C	-2.24	-1.11
Pd@Nb_2C	-1.94	-1.10
Ag@Nb_2C	-2.40	-1.12

Table S3. N–N (d_{N-N}) and C–O (d_{C-O}) bond lengths (Å) for N_2 and CO co-adsorbed on Nb_2C and TM@Nb_2C.

System	d_{N-N}	d_{C-O}
Nb_2C	1.296	1.233
Sc@Nb_2C	1.304	1.238
Ti@Nb_2C	1.338	1.234
V@Nb_2C	1.328	1.236
Cr@Nb_2C	1.311	1.241
Mn@Nb_2C	1.301	1.234
Fe@Nb_2C	1.293	1.233
Co@Nb_2C	1.286	1.234
Ni@Nb_2C	1.292	1.236
Cu@Nb_2C	1.303	1.240
Zr@Nb_2C	1.307	1.248
Mo@Nb_2C	1.318	1.232
Ru@Nb_2C	1.280	1.235
Rh@Nb_2C	1.260	1.256
Pd@Nb_2C	1.329	1.237
Ag@Nb_2C	1.300	1.245

Table S4. Calculated adsorption energy of $*N_2$ and *CO in their co-adsorption state (eV) on Nb_2C and TM@Nb_2C.

System	N_2	CO	Difference
Nb_2C	-2.22	-2.08	-0.14
Sc@Nb_2C	-2.55	-2.21	-0.34
Ti@Nb_2C	-2.57	-2.43	-0.14
V@Nb_2C	-2.71	-2.63	-0.08
Cr@Nb_2C	-2.66	-2.49	-0.17
Mn@Nb_2C	-2.30	-2.18	-0.12
Fe@Nb_2C	-2.62	-2.12	-0.50
Co@Nb_2C	-2.47	-2.17	-0.30
Ni@Nb_2C	-1.91	-1.87	-0.04
Cu@Nb_2C	-1.96	-1.76	-0.35
Zr@Nb_2C	-2.63	-2.21	-0.42
Mo@Nb_2C	-2.34	-1.98	-0.36
Ru@Nb_2C	-2.39	-2.01	-0.38
Rh@Nb_2C	-2.24	-1.93	-0.31
Pd@Nb_2C	-1.94	-1.79	-0.15
Ag@Nb_2C	-2.40	-2.08	-0.32

References

1 J. A. Dean, *Lange's Handbook of Chemistry*, McGraw-Hill, New York, 15th edn, 1999.

2 D. W. Smith, *J. Chem. Educ.*, 1977, **54**, 540.

3 P. J. Linstrom and W.G. Mallard, *NIST Chemistry WebBook*, NIST Standard Reference Database Number 69, National Institute of Standards and Technology, Gaithersburg MD, https://doi.org/10.18434/T4D303, (accessed March 25, 2026).